**Light Metals 2014**
*Edited by: John Grandfield*
***TMS (The Minerals, Metals & Materials Society), 2014***

# NUMERICAL SIMULATION OF FULL LIFE CYCLE CATHODE ASSEMBLY PERFORMANCES FOR DESIGN OPTIMIZATION

Guorong Cao[1], Xinquan Zhang[2], Hao Zhang[1]
[1]Pacific Aluminium Services, Level 3 /500 Queen St Brisbane, Qld. 4000, Australia
[2]Research Avenue, Bundoora, Vic. 3083, Australia

Keywords: aluminum smelting, cathode, modeling

## Abstract

The importance of the cathode assembly thermal-electrical and thermal-mechanical performance cannot be overstated when designing an aluminum reduction cell. However, it is extremely difficult to measure in-service cathode assembly performance or to infer in-service behaviour from any measurements of cathode assemblies at room temperature. A complete thermo-electrical and thermo-mechanical modelling approach has been developed to conduct sequentially coupled simulation of the cathode assembly lifecycle performance. The modelling starts with the cathode rodding process which allows the air gap between the cast iron and carbon to be predicted. The results are built into the subsequent thermo-electrical and thermo-mechanical models of the in cell operation. The cathode voltage drop is then estimated by coupling the predicted contact pressure and temperature with the electrical contact resistance. The model predicted air gaps as well as cathode voltage drop savings due to design changes have been validated by carefully designed experimental measurements for various cathode assembly designs.

## Introduction

The cathode assembly is a core part of a reduction cell. Optimization of the cathode assembly design should study the impact of the contact pressure and temperature on electrical resistance between the cathode and the cast iron as well as mechanical stress inside the cathode which could lead to cathode cracking. Richard [1] developed a semi-empirical constitutive equation linking contact pressure and temperature between carbon and cast iron to electrical contact resistance by calibrating a numerical model against Sørlie's experiment results [2]. Dupuis [3] presented a thermo-electrical mechanical model for the design optimization of cathode collector bar slots. The model applied the estimated temperature profiles of the cathode assembly at the moment the cast iron fills the slots. The thermal mechanical behavior of the cathode assembly as it reached a thermal profile of an operating cathode assembly was then simulated. This approach did not simulate the impact of plastic deformation and phase transformation of the cast iron during cathode casting. Blais [4] described the application of finite element models for optimal cathode shape design for energy saving while Gagnon [5] developed a thermo-electro-mechanical finite element model of cathode assembly with analytically calculated air gaps between cast iron/cathode interfaces for design optimizations. The present model simulates the cathode assembly from cathode casting right through to in-cell operations, allowing accurate prediction of the air gap formation during casting and its impact on the life cycle performance of cathode assemblies.

## Finite Element Models

A commercial FEM package ABAQUS was used for the models. The following steps were taken to model the life cycle performances of a cathode assembly:

- Set up and calibration of the transient thermal model of the cathode casting process. The calibration was performed using temperature measurements from embedded thermocouples during a controlled cathode casting experiment.
- Calibration of the sequentially coupled thermal-mechanical model of the cathode casting and cooling processes against experimental measurements. These calibrated models were then used to examine the stress distribution inside the cathode and the size of air gaps between the cast iron and the cathode.
- Merging the cathode assembly model to a half cathode reduction cell thermal mechanical model with the exact air gap sizes that have been predicted by the model. A steady state thermal mechanical model was carried out using cell operating temperature as the thermal loading condition to predict the maximum principal stress in the cathode and the contact pressure between cast iron and the cathode.
- A final half cathode thermal electrical model with contact electrical resistance linked to contact pressure and temperature between the cast iron and the cathode was used to predict the cathode voltage drop during the cell operation and cell thermal electrical performances. An in-house developed ABAQUS user subroutine was used to define the contact electrical resistance as a function of contact pressure and temperature.

Figure 1 shows the mesh of the finite element model for the transient thermal and sequentially coupled thermal mechanical analysis of the cathode casting process. Due to symmetry, only one quarter of the cathode assembly was modeled. Coincident nodes were used for contact surfaces between the cast iron/cathode and cast iron/bar interfaces. The cathode is 505 mm in width and 450 mm in height while the collector bar is 170 mm in width and 150 mm in height.

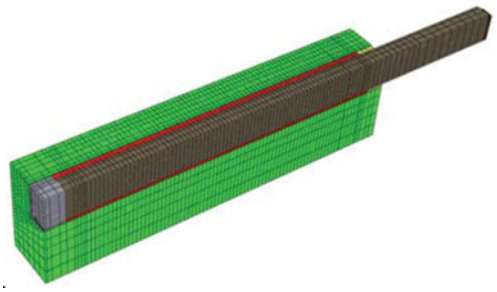

Figure 1. FE mesh of a cathode assembly for thermal-mechanical modeling of the casting and cooling processes.

The cathode assembly model has been merged with a cell thermal-electrical and mechanical model with model predicted air gaps built into the cast iron and cathode contact surfaces (Figure 2). This integrated model has been used to simulate in-cell thermal-mechanical and thermal-electrical performances of the cathode assembly.

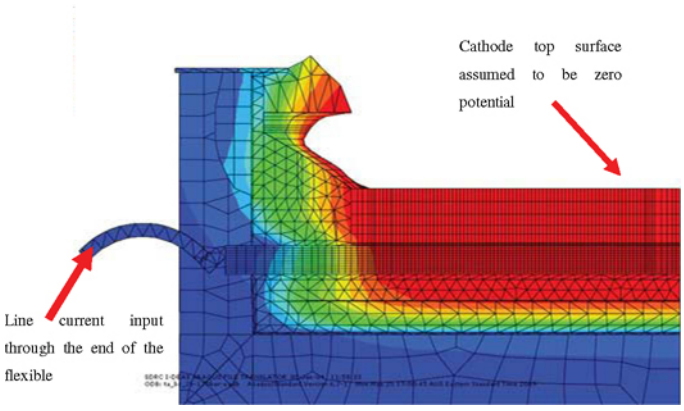


Figure 2. The integrated model for simulation of in-cell thermal-mechanical and thermal-electrical performances of the cathode assembly.

The boundary conditions used for the cathode casting thermal analysis are listed below:

- The initial casting temperature of the cast iron was set at 1375 $^0$C and it was assumed that the cast iron filled the gap instantaneously, i.e., the filling process was not modeled. A temperature profile was applied to the cast iron to simulate its temperature change during the filling process. A pre-heat temperature range of 530 $^0$C to 630 $^0$C was used for the bar while a pre-heat temperature range of 270 $^0$C to 350 $^0$C was assumed for the cathode based on the plant trial. The temperature field obtained after the initial air-cooling simulation of the bar and cathode was used as the initial temperature for the transient casting analysis.

- Convection and radiation boundary conditions were applied to all exposed surfaces. Thermal contact resistances were determined by the model calibration for the contact surfaces between bar/cast iron and cast iron/cathode.

The boundary conditions for the stress analysis are as follows:

- Gravitational force was applied to all the parts. The out-of-plane degree of freedom was constrained in the plane of symmetry. The cathode was supported by rigid surfaces during casting while the cell cradle was supported at the bottom for thermo-mechanical modeling of the cell operation.

- Mechanical contacts between various parts in the model were simulated by using a friction factor of 0.1 and elastic slip factor of 0.15. For the cell operation model, the side of the cathode was un-constrained to simulate the end stall cathode that is usually under much less compressive load from the end wall lining.

**Plant Trial**

A plant trial of casting two graphitized cathode assemblies was conducted in a cathode preparation plant. The temperature history was monitored during the casting and cooling processes by 21 embedded thermocouples as shown in Figures 3 and 4. The cathode assembly was then sectioned at 4 locations to measure the air gap size at the room temperature as shown in Figure 5. Displacements of the bar and cathode were also measured using dial gauges and filmed using video cameras during cathode casting process for the model calibration (Figure 6).

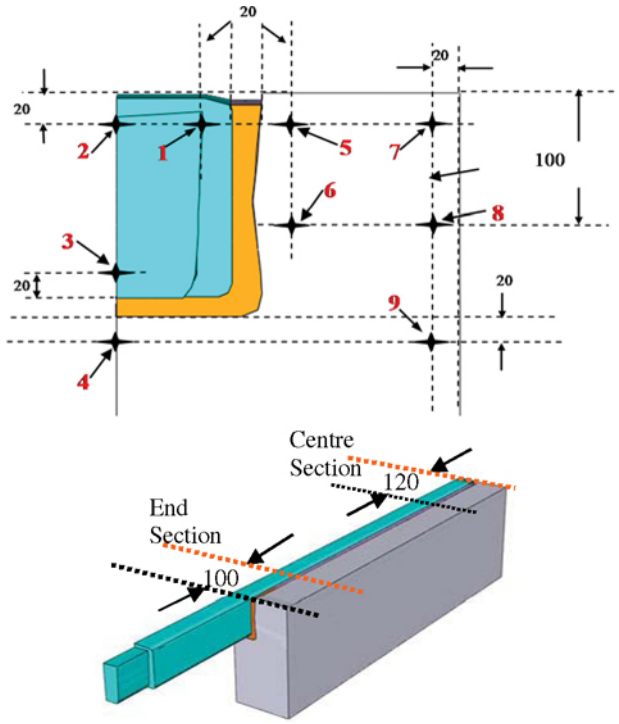


Figure 3. Thermocouple locations during the trial (only 1/4 of the assembly was shown).

Figure 4. Temperature measurements during the plant trial.

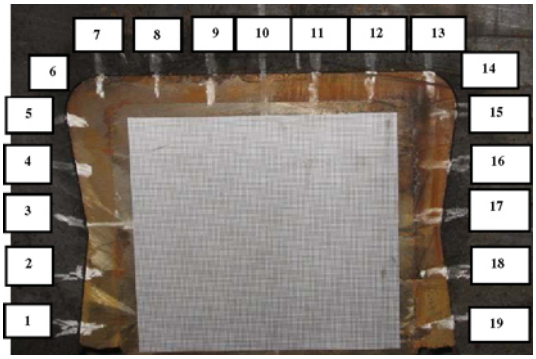


Figure 5. Locations of air gap measurements.

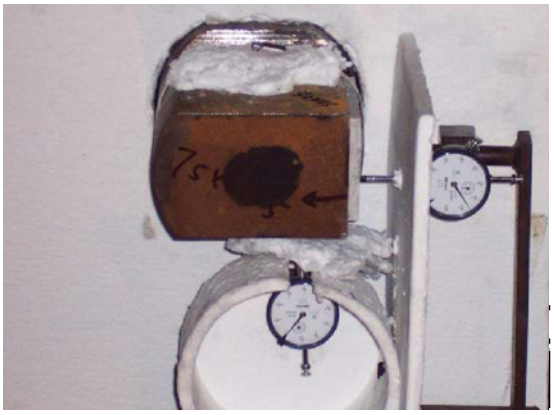

Figure 6. Displacements of the bar and cathode were also measured during the cathode casting process for the model calibration.

## Model Calibration

The predicted temperatures are compared with the plant measurements in Figures 7 and 8. Good agreements between the modeled temperature history and the measured temperature history have been achieved.

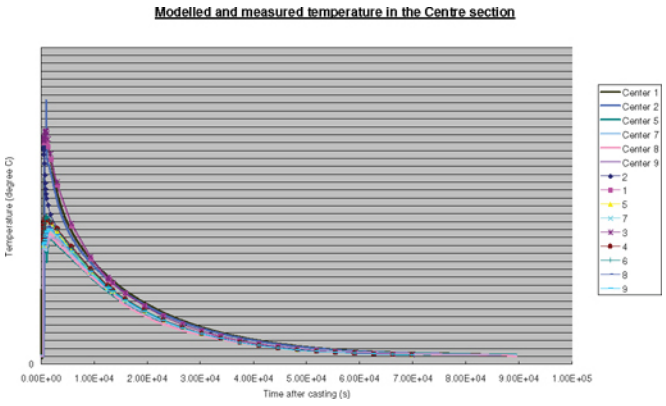


Figure 7. Comparison of modeled and measured temperatures in the center section, (lines with marks are model predictions).

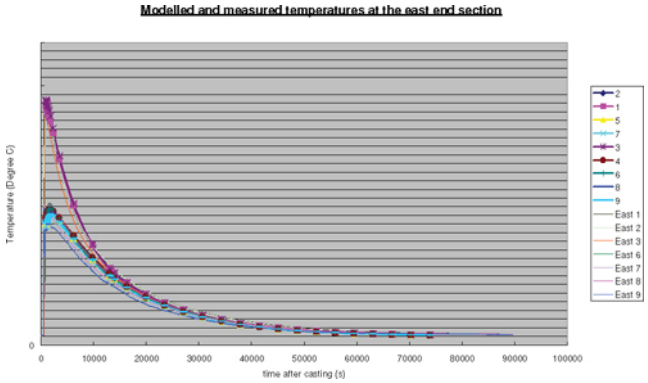


Figure 8. Comparison of modeled and measured temperatures in the end section, (lines with marks are model predictions).

## Air Gap Prediction

Air gaps formed between the cast iron and cathode were measured using a filler gauge at various cross-sections during the plant trial after the cathode casting process and the assembly was cooled to room temperature. Figure 9 compares the modeled and measured air gap sizes at the end section for measured positions shown in Figure 5. It can be seen that a good agreement has been achieved. Figure 10 shows a contour plot of the air gap predicted by the model for the cast iron and cathode contact surface. Generally the air gaps on two sides of the slot (positions 1 to 6 in Figure 5) are smaller than that of the bottom of the slot (positions 7 to 10), which is consistent with the air gap measurements.

The maximum principal stress inside the cathode during the cell operation was predicted by the cell thermal mechanical model with air gaps between the cast iron and cathode built into the model. Figure 11 shows the distribution of the maximum principal stress in the cathode. The maximum principal stress can be used for comparative studies to compare the risk of cathode cracking for various designs, especially to those so called known safe designs in our smelters.

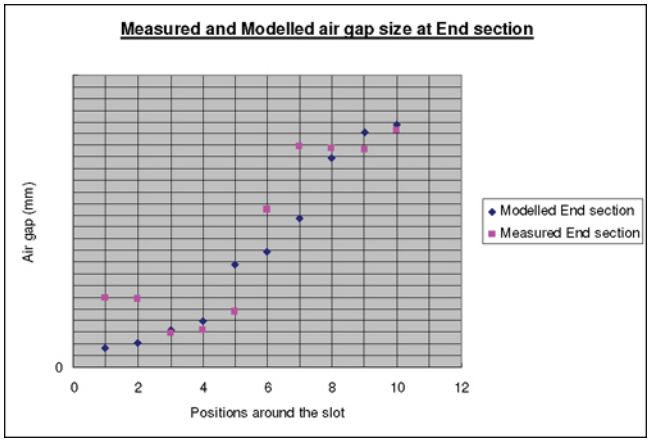


Figure 9. Comparison between the measured and modeled air gap sizes at the end section.

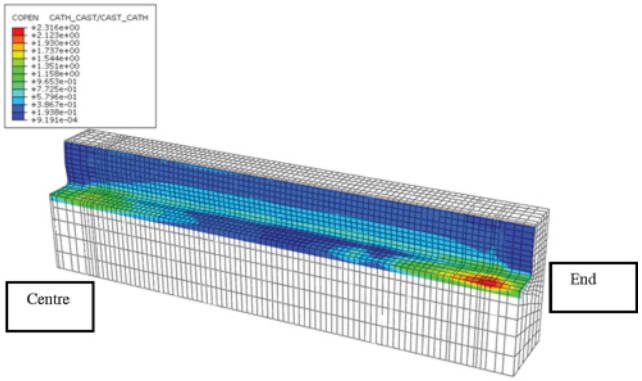


Figure 10. A contour plot of the predicted air gap sizes between the cast iron and the cathode at the room temperature after cathode casting (one quarter cathode model due to symmetry).

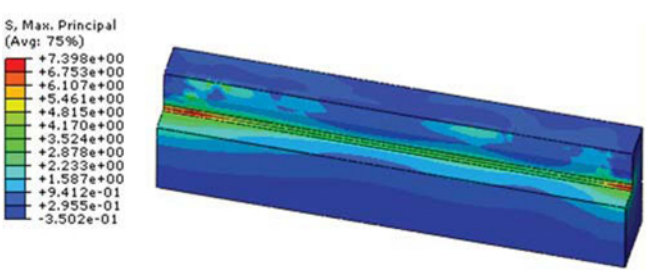


Figure 11. The distribution of the maximum principal stress in the cathode.

### Case Studies and Discussions

The calibrated models have been used for a number of parametric studies to determine the impact of various design parameters. Table I shows a case study on the impact of the centre dam length and end-insulation length on the cathode voltage drop, the cathode surface current density and the maximum principal stress in the cathode during the cathode casting and cell operation.

Table I. Cathode assembly configuration cases.

| Cases | Centre dam (mm) | End insulation (mm) |
|---|---|---|
| 1 (base case) | 200 | 90 |
| 2 | 100 | 90 |
| 3 | 75 | 90 |
| 4 | 200 | 150 |
| 5 | 100 | 150 |
| 6 | 75 | 150 |
| 7 | 75 | 180 |
| 8 | 100 | 50 |
| 9 | 200 | 50 |

The results show that the end insulation length has a significant impact on cathode voltage drop while the center dam length does not appear to have a significant impact on cathode voltage drop as shown in Figure 12. Reducing the center dam length from the base case of 200 mm to 100 mm and 75 mm while keeping the end insulation at 90 mm have no impact on cathode voltage drop. However, for the two cases where the end insulation length is reduced to 50 mm, there is a 4 mV reduction in the cathode voltage drop if the center dam length is reduced from 200 mm to 100 mm. There is a voltage saving of 6 mV if the end insulation length is reduced from 90 mm to 50 mm in the base case as indicated by comparing case 1 and case 9. Conversely, there will be a voltage penalty of 10 and 30 mV respectively if the end insulation is increased from 50 mm to 90 mm and 150 mm respectively while keeping the center dam length at 100 mm. Similar results can be seen for three cases with 75 mm center dam length, in which the voltage drop is increased by 20 mV and 27 mV respectively as the end insulation is increased from 90 mm to 150 mm and 180 mm. The model predicted voltage distributions in 3 of the studied cases are shown in Figure 13 as examples.

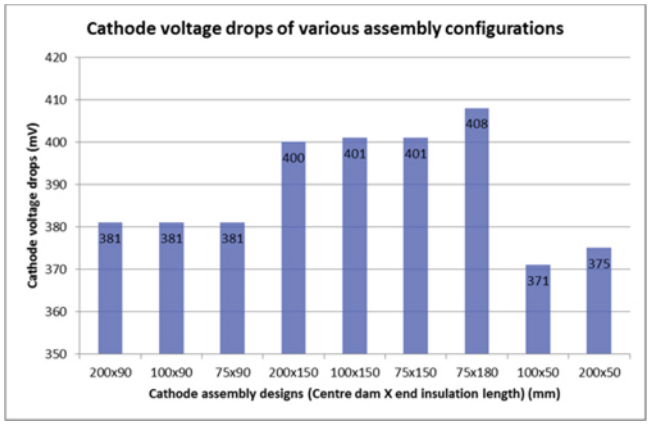


Figure 12. Cathode voltage drops for various assembly configuration cases as listed in Table I. Case 1 is the base case.

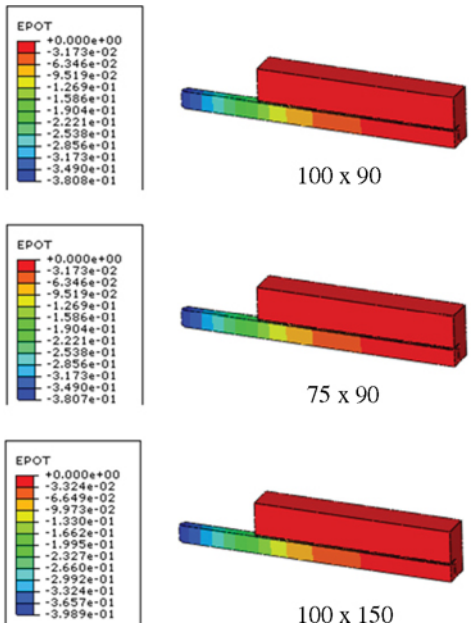


Figure 13. Cathode voltage drops predicted by the model, text box indicating the center dam and end insulation length.

The center dam and end insulation length have appreciable impact on the current density of the cathode surface especially near the end of the cathode towards the side wall as shown in Figure 14.

Reducing the center dam length and increasing the end insulation have resulted in a more even current distribution between the center of the cathode and the end of cathode although the current flow is still heavily biased towards the end of the cathode as the current always takes the least resistive path. Increasing the end insulation has the effect of shifting the highest current density away from the end of the cathode. The highest current density area reduces as the center dam length reduces for cases that have the same end insulation. It should be emphasized that diverting the current away from the least resistive path will result in a voltage penalty.

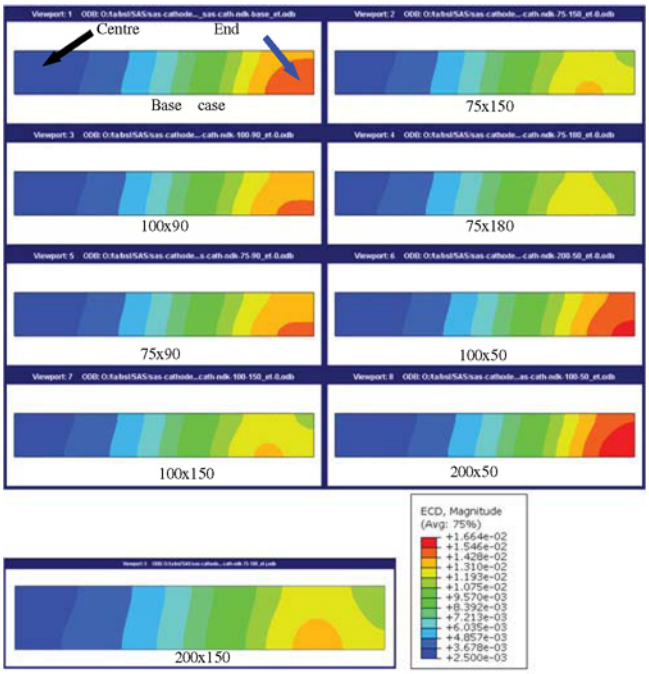


Figure 14. Current density distributions on the cathode surface for various assembly configuration cases as listed in Table I. Only 1/4 of the cathode is shown due to the assumption of symmetry.

The distribution of the maximum principal stress in the cathode of various designs at around 32 seconds after casting when the stress reached the highest level is shown in Figure 15. The highest maximum principal stress is always located at the end of the cathode and at the corner of the slot. This is caused by the interaction between the collector bar and cast iron during the casting process. The bar displacement interacts with rapidly solidifying cast iron, resulting in high maximum principal stresses in the cathode. Figure 16 compares the stress levels reached in each of the cases studied and it can be seen that the end insulation length has a significant impact on the maximum principal stress level. The longer the end insulation, the higher the maximum principal stress will be in the cathode among the studied cases, contrary to the single collector bar assembly. Another unique result for the split bar design is that there is another high stress zone in the cathode near the centre end of the bar at around 200 seconds after casting as shown in Figure 17. However, these stress levels are not as high as those shown in Figure 15 and the fact that this zone is near the centre of the cathode also means that the risk of cathode cracking is lower than the high stress zone near the end of the cathode. It is important to note that the high stress level among these cases is due to the assumption of elastic material property for the cathode in the model rather than the use of elastic-plastic properties.

During the case study, the formation of air gaps between the cast iron and cathode after the cathode casting was also simulated. Figure 18 shows the predicted air gaps in three of the studied cases. It can be seen from Figure 18 that the air gap sizes are not uniform between the cast iron and cathode at about 26 hours after casting.

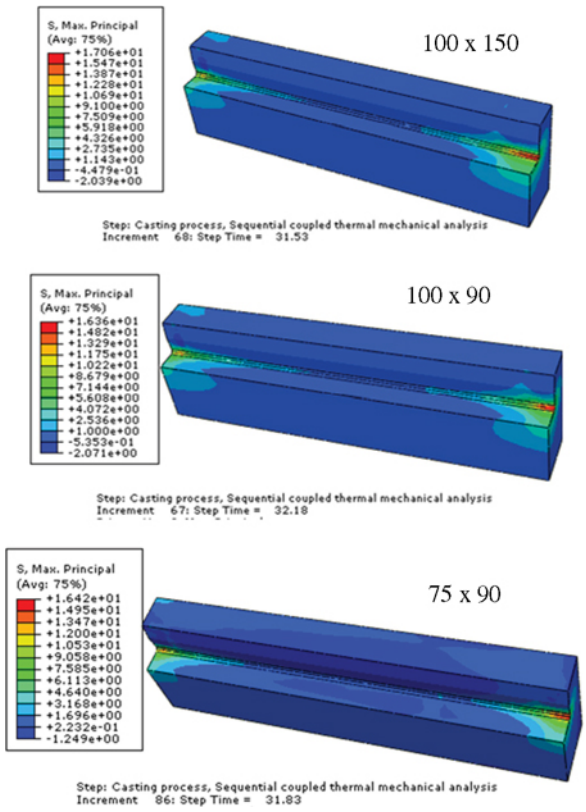


Figure 15. Distribution of maximum principal stress in the cathode at around 32 seconds after casting when the stress reached the highest level at the end of the cathode.

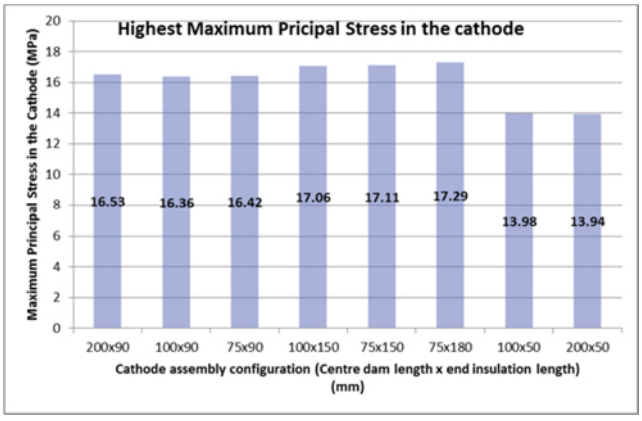


Figure 16. Predicted maximum principal stress in the cathode during casting process for the cases listed in Table I.

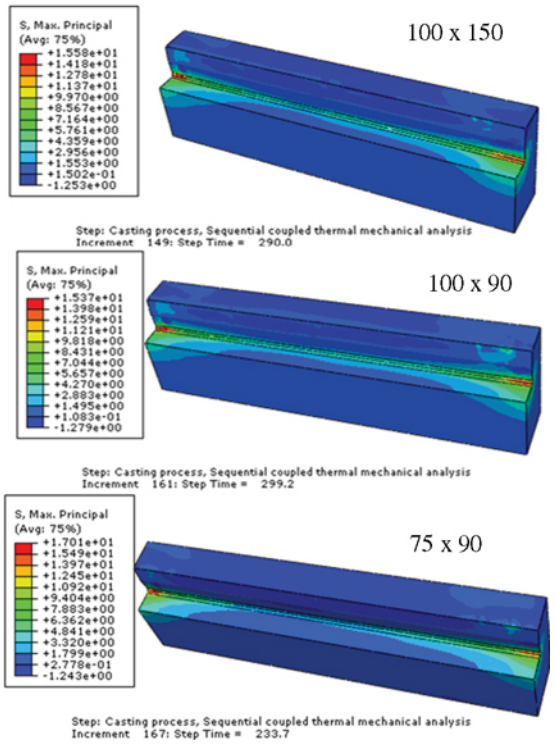


Figure 17. Distribution of the maximum principal stress in the cathode at more than 235 seconds after casting when the stress reached the highest level near the centre of the cathode.

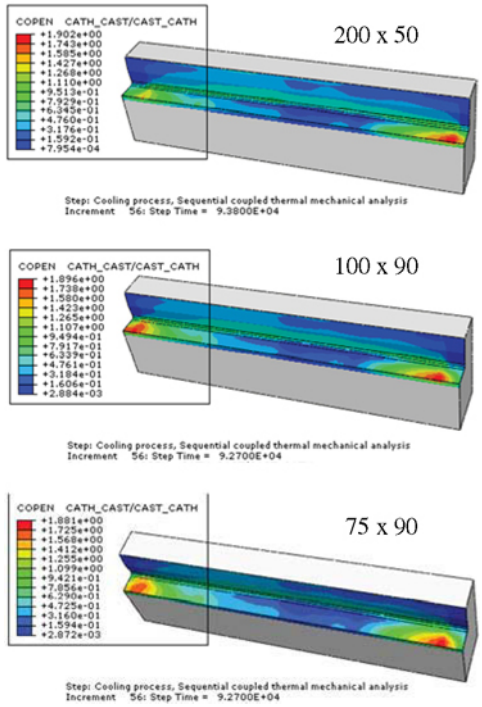


Figure 18. Air gap distributions between the cast iron and cathode after the cathode casting and the cathode assembly is cooled to room temperature.

## Conclusions

Comprehensive thermal electrical and thermal mechanical finite element models have been developed to simulate the lifecycle performance of cathode assemblies for design optimization. Carefully planned plant trials have been conducted to calibrate the model. The case studies presented in the paper demonstrate that detailed comparative studies on the cathode thermal electrical and thermal mechanical performance can be achieved using these models. This approach has been applied to a number of cathode assembly design optimization studies over the last 10 years with a high rate of success. Cast iron filling and solidification processes have not been modeled in the current model therefore casting conditions that could lead to various casting defects cannot be studied using the current approach. In addition, other cathode performance issues, such as the cathode erosion mechanism, the impact of sodium expansion and the initiation and propagation of cathode cracking, should be studied separately.

## References

[1] D. Richard, "Thermo-electro-mechanical modeling of the contact between steel and carbon cylinders using finite element method," *Light Metals 2000*, p. 523-528.

[2] M. Sørlie, "Cathode collector bar-to-carbon contact resistance," Light Metals 1992, p. 779-787.

[3] M. Dupuis, "Development and application of an ANSYS based thermo-electro-mechanical collector bar slot design tool," *Light Metals 2011*, p. 519-524

[4] M. Blais, "Energy saving in Aluminum electrolysis: effect of the cathode design," *Light Metals 2013*, p. 627-631

[5] M. Gagnon, "Optimization of the cathode collector bar with a Copper insert using finite element method," *Light Metals 2013*, p. 621-626

## Acknowledgement

The author would like to thank the following existing and former staff members of Pacific Aluminium: Graham Paterson, Tseng Khoo and Donald Walker for their contribution in carrying out cathode casting trials and measurements.